PRELIMINARY NOTES

An Investigation of a Double-Tracer Technique for Positron Computerized Tomography

S. C. Huang, R. E. Carson, E. J. Hoffman, D. E. Kuhl and M. E. Phelps

UCLA Medical School, University of California, Los Angeles, California

We describe a double-tracer technique for positron computed tomography (PCT) that utilizes the difference in physical decay rates to distinguish between two positron emitters. The technique is applied to PCT studies on phantoms (a) to separate two tracers with different half-lives, and (b) to measure simultaneously the attenuation coefficients and the tracer concentrations in a phantom. Results from these experiments are encouraging, but they also reveal a major limitation of the technique, namely, noise enhancement that is related to the relative half-lives of the two tracers and the time duration of the PCT scans, as well as to the relative concentrations of the two tracers. If these parameters are carefully selected, the double-tracer technique will have high potential for examining simultaneously two different biological processes with PCT and for measuring tracer concentrations and attenuation correction factors at the same time.

J Nucl Med 23: 816–822, 1982

In nuclear medicine, double-tracer techniques have been used with scanners (*1*,*2*) and with gamma cameras (*3*–*5*) to image simultaneously the distributions of two radiotracers in the body. In these techniques, two tracers labeled with nuclides having sufficiently different photon energies are introduced in the patient, and the separation of the two tracers is achieved by energy discrimination. Because the two tracers are in the body at the same time and are measured simultaneously, the double-tracer techniques can reduce the problems of patient movement, image alignment, and physiologic changes, all unavoidable if the two tracers are imaged successively.

In addition to the above advantages, double-tracer techniques can also be used to measure photon attenuation and tracer distribution simultaneously in positron computerized tomography (PCT). This application could reduce the artefacts due to patient movement between the measurements of attenuation correction factors and the tracer distribution (*6*). However, since photons emitted from the annihilation of positrons have the same energy (511 KeV), the technique of energy discrimination is not applicable to positron emitters. We have investigated a method that monitors decay in several PCT projections to separate two positron emitters by utilizing their different decay rates. Preliminary results reported here are promising. Some potential problems are also discussed.

Received Feb. 18, 1982; revision accepted May 3, 1982.

For reprints contact: Dr. Sung-cheng Huang, Div. of Biophysics, Dept. of Radiological Sciences, UCLA Medical School, 405 Hilgard Avenue, Los Angeles, CA 90024.

THEORY

In a cross section containing two positron emitters, A and B, let their distribution at time t be denoted as $f_A(x,y,t)$ and $f_B(x,y,t)$ respectively, where x,y are the spatial coordinates in the section. Allowing for physical decay of the nuclides, the distribution of the combined positron-emitting radioactivity in the cross section at time t is

$$f(x,y,t) = f_A(x,y,0)e - \lambda_A t + f_B(x,y,0)e-\lambda_B t \quad (1)$$

where λ_A and λ_B are the decay constants of the two emitters. At any time t, the attenuation-corrected pro-

jection of the distributions along a line $l(r,\theta)$, which has a perpendicular distance r from the center and makes an angle θ with the x axis, can be denoted by the following line integral.

$$m(r,\theta,t)$$

$$= \int_{l(r,\theta)} [f_A(x,y,0)e^{-\lambda_A t} + f_B(x,y,0)e^{-\lambda_B t}]ds \quad (2)$$

$$= m_A(r,\theta)e^{-\lambda_A t} + m_B(r,\theta)e^{-\lambda_B t} \quad (3)$$

where $m_A(r,\theta)$ and $m_B(r,\theta)$, both independent of time, denote respectively the line integrals of $f_A(x,y,0)$ and $f_B(x,y,0)$. Thus the time function of the projection $m(r,\theta,t)$ consists of two exponential components with time constants $(1/\lambda)$ derived from the decay constants of the two nuclides while the coefficients of these exponential components are the projections of the corresponding individual distributions at zero time. According to the theory of computerized tomography (CT), the $f_A(x,y,0)$ and $f_B(x,y,0)$ can be reconstructed from their projections $m_A(r,\theta)$ and $m_B(r,\theta)$ (*7,8*). Therefore, if the coefficients of the two exponential terms can be estimated from the time function of each projection measurement $m(r,\theta,t)$, the individual distributions f_A and f_B can be obtained from CT reconstruction of the estimated coefficients.

Because the decay constants λ_A and λ_B are known, estimates of the coefficients m_A and m_B from the time function of $m(r,\theta,t)$ can be obtained, in a single step, by the following estimation equations (see Appendix)

$$\hat{m}_A = \frac{1}{D}\left[\left(\sum_i z_i e^{-\lambda_A t_i}\right)\left(\sum_i e^{-2\lambda_B t_i}\right) - \left(\sum_i z_i e^{-\lambda_B t_i}\right)\left(\sum_i e^{-(\lambda_A+\lambda_B)t_i}\right)\right]$$

and

$$\hat{m}_B = \frac{1}{D}\left[\left(\sum_i z_i e^{-\lambda_B t_i}\right)\left(\sum_i e^{-2\lambda_A t_i}\right) - \left(\sum_i z_i e^{-\lambda_A t_i}\right)\left(\sum_i e^{-(\lambda_A+\lambda_B)t_i}\right)\right],$$

where

$$D = \left(\sum_i e^{-2\lambda_A t_i}\right)\left(\sum_i e^{-2\lambda_B t_i}\right) - \left(\sum_i e^{-(\lambda_A+\lambda_B)t_i}\right)^2 \quad (4)$$

and $z_i = m(r,\theta,t_i)$ is the measured projection value at time t_i. This estimation is required for every projection (at all values of r and θ).

When attenuation and tracer distribution are to be measured simultaneously, the separation procedure is the same, except that (a) the attenuation correction is not needed for $m(r,\theta,t)$, and (b) one of the estimated coefficients (e.g., $\hat{m}_A$) is the projection of the tracer distribution without attenuation correction, while the other ($\hat{m}_B$) corresponds to a transmission measurement. The latter would provide the attenuation-correction factors (ACF) that are then applied to the other estimate ($\hat{m}_A$) to reconstruct an attenuation-corrected distribution of tracer in the cross section.

MATERIALS AND METHODS

Projection data were measured using either an ECAT II* (9) or a NeuroECAT* (*10*). In order to find the time function of each projection, the standard ECAT II/NeuroECAT data-collection software was modified to save all the raw counts and collection-time data for each coincidence detector pair. The raw counts were later normalized for detection efficiency and sorted according to their projection positions. On the NeuroECAT, the scanning was done with 5.55-mm linear and 1.875° angular sampling and without shadow shields. For a typical 3-min scan, the measurement-time resolution is 16.4 sec for projections near the center ($r \sim 0$), and averages 36 sec for projections at a distance r = 6.5 cm from the center. For ECAT II we used the standard shadow shield (2.29-cm opening) and standard sampling (5.71-mm linear and 2.5° angular). For a 3-min scan, the measurement-time resolutions are 16.4 sec and 26 sec respectively for projections at r = 0 and r = 6.5 cm. For each measured time function of the projections, the coefficients $\hat{m}_A$ and $\hat{m}_B$ were estimated according to Eq. 4.

In two studies, the double-tracer technique was applied to separate two positron emitters in a phantom. In a third study the technique measured simultaneously the attenuation and radioactivity distribution of a phantom. ECAT II/NeuroECAT's reconstruction software with medium reconstruction filter (*9,10*) was used for PCT image reconstructions.

In the first study we used a three-compartment water phantom with a diameter of 17.8 cm (Fig. 1). The center compartment was filled with 9.8-min N-13 ammonia (about 0.8 μCi/ml) while the two adjacent compartments contained 109.8-min F-18 fluorodeoxyglucose (FDG) (about 0.5 and 0.4 μCi/ml). Four 3-min NeuroECAT scans were then started at 0, 3, 6 and 15.5 min, giving a total of 6 million counts. After correction for attenuation using the geometric method, m_A and m_B were estimated from the time function of the non-decay corrected projection data and were reconstructed to give the individual distributions of N-13 and F-18. Regular PCT images of the four scans were also reconstructed (assuming F-18 for decay correction). After 90 min, when most of the N-13 had decayed, the phantom was rescanned (20 min, 2.6 million counts) to give a control image of the F-18 tracer.

Another phantom (diam 20 cm, Fig. 4) with six separate compartments was filled with 68.3-min Ga-68 and 12.7-hr Cu-64, with specific activities about equal. It was then positioned in an ECAT II scanner. Five 10-min

scans were made in sequence (50 million counts total) to obtain the measured time functions of the projections, and the double-tracer technique was applied. Attenuation correction was done with the geometric method. After 24 hr, when most of the Ga-68 had decayed, the phantom was rescanned (10-min, 2.3 million counts) to give a control Cu-64 image.

In the third study, which measured simultaneously the ACFs and radioactivity concentrations, the transmission ring of NeuroECAT was filled with Ga-68 solution (~5 mCi) and a reference transmission scan was made (28 million counts) without phantom in place. The two side compartments of the phantom used in the first study were filled with different N-13 (T 1/2 = 10 min) ammonia solutions (~0.04 and ~0.3 μCi/ml), while the center compartment contained water. An emission scan of the phantom (3 min, 1.1 million counts) was made with the transmission ring source temporarily removed, and geometric attenuation correction was used to reconstruct a control image of the N-13 ammonia distribution in phantom. Immediately afterward, the water in the center compartment was drained, the transmission ring source (Ga-68) was placed in the NeuroECAT, and seven 3-min double-tracer scans were obtained, collecting 21 million counts in all. An hour after the start of the double-tracer scans (with <2% of the N-13 remaining), a transmission scan of the phantom was obtained (20 min, 9.6 million counts) to give a control image of the attenuation coefficients in the phantom. The time functions of the projection measurements collected during the seven 3-min double-tracer scans were used by the double-tracer technique to separate the Ga-68 in the ring source from the N-13 in the phantom. An image of the attenuation coefficients corresponding to the separated Ga-68 measurement was reconstructed to compare with the control transmission image. The separated N-13 radioactivities were reconstructed by using (a) the ACFs derived from the double-tracer technique, then (b) those from the control transmission scan. These N-13 ammonia images were compared qualitatively and quantitatively with the control N-13 image.

RESULTS

Figure 1 shows a sequence of four PCT images of a phantom containing N-13 and F-18. The shorter half-life of N-13 is signalled by the faster fade-out in the middle compartment. The measured time function of a projection near the center at $\theta = 90°$ is shown in Fig. 2. The F-18 and N-13 images as separated by the double-tracer technique are shown in Fig. 3. The pixel-by-pixel sum of the two images is shown to be qualitatively similar to the first PCT image in Fig. 1. The F-18 image was found to be similar to the F-18 control image taken at 90 min. Quantitative values from the separated F-18 image also

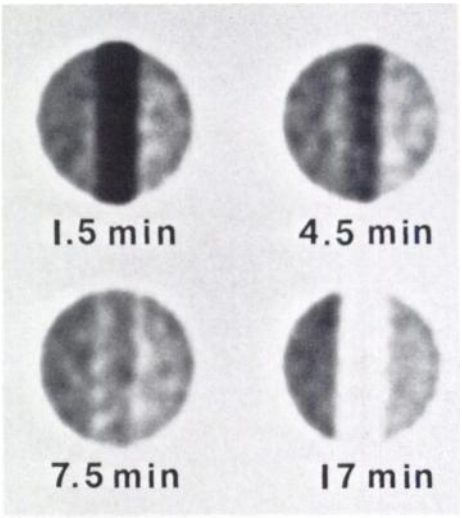

FIG. 1. Sequence of four regular 3-min PCT images of a phantom with three separate compartments. Center compartment contained N-13 ammonia solution and two side compartments held different concentrations of F-18 FDG solution. Time under each image is mid time of scan. Shorter half-life of N-13 is revealed by faster fading in center compartment.

match those of the control F-18 image, as shown in Table 1. The separation between F-18 and N-13 is also shown in Table 1 to be nearly complete: small values in the F-18 compartment of the N-13 image and vice versa. The quantitative value in the N-13 compartment of the sum image (Table 1) is slightly higher than that for the initial image, due to the use of F-18 half-life for decay correction in the reconstruction of the initial image, which underestimates the N-13 radioactivity.

Results of the second study are shown in Fig. 4. The radioactivities of Ga-68 and Cu-64 are clearly separated by the technique (see Table 1). The sum of the two separated images is indistinguishable from the PCT image taken at time zero (not shown). The Plexiglas partitions

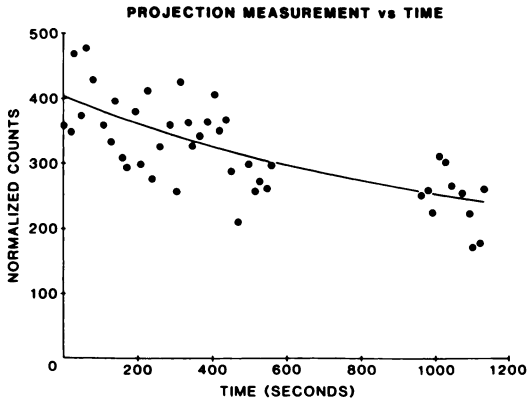

FIG. 2. Plot of time function of a PCT projection measurement collected from four scans shown in Fig. 1. Dots are actual projection measurements used to estimate separate F-18 and N-13 radioactivities from Eq. 4. Curve is generated from resultant estimates using Eq. 3. Projection measurements were taken at $\theta = 90°$ and r ~3 cm.

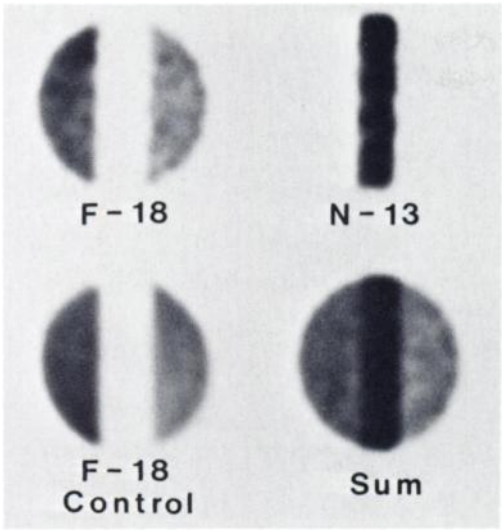

FIG. 3. Images of F-18 and N-13 as separated by double-tracer technique (top). Clean separation is shown. F-18 image is further shown to be similar to control F-18 image taken at 90 min (lower left), when <0.2% of the N-13 remains. Lower right image is direct sum of separated F-18 and N-13 images. Its similarity to the 1.5-min image in Fig. 1 supports correctness of N-13 image as separated by double-tracer technique.

(3 mm thick) separating the compartments in the phantom are also visible in the sum image, and they cause the two Cu-64 spots to look smaller than the corresponding voids in the Ga-68 image. The Cu-64 image and its control image are similar, although there is more noise in the double-tracer image. Quantitative comparisons between the separated Cu-64 and the control Cu-64 images, and between the sum image and the initial image, again confirm the correctness of the double-tracer technique.

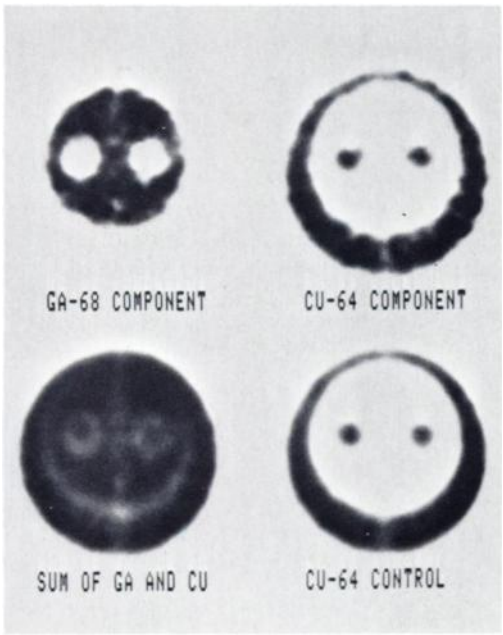

FIG. 4. Second phantom experiment: five 10-min scans with Ga-68 and Cu-64 in separate compartments. Top images show distributions as separated by double-tracer technique. At lower right control Cu-64 image (made 24 hr later) confirms true Cu-64 distribution in phantom. Direct sum of separated Cu-64 and Ga-68 images (lower left) is found similar to the first 10-min PCT image (not shown) of phantom.

Resultant images of the combined transmission and emission scans are shown in Figs. 5 and 6. The attenuation-coefficient image as obtained by the double-tracer technique is similar to the one from the control transmission scan (Fig. 5). The attenuation coefficients for water, as obtained from the two images, are both ~0.090 cm^{-1} (Table 1), which is consistent with values previously obtained (*11*,*12*).

The N-13 images obtained by the double-tracer technique are shown in Fig. 6. Attenuation correction was performed using ACFs, derived either from the double-tracer technique or from the control transmission scan. There is a small difference in noise level between the two images. The true radioactivity distribution as obtained from the control N-13 scan is also shown in the figure for direct comparison. The two images by the double-tracer technique are much noisier than the control (Table 1 shows their CVs to be about 30% and 23% compared with 5% in the control). Quantitative comparison of the N-13 concentrations among the three images in Fig. 6 shows some small differences, which by Student's t-test were not significant because of the high noise levels. However, the value from the control image is expected to be higher than the values from the other two N-13 images, because the transmission-ring source, which included a 1/4-inch-thick plastic support, was removed during the N-13 control scan, whereas during the double-tracer scan the ring added extra attenuation to the photons from N-13. By scanning a phantom both with and without the ring (no radioactivity) in place, the loss due to the ring was found to be ~9%. This attenuation can be calibrated and incorporated into the normalizing procedure for the detector efficiency of a PCT scanner.

For the three studies reported, the data processing required to separate the two tracers took 5 to 10 min per study on a computer, depending on the number of scans in the study. A large fraction of this time is needed to sort the raw data into proper time sequences of the projection measurements. With some modifications in the ECAT II/NeuroECAT data-collection programs, it is possible to sort the projection data during collection, and the processing time can be much reduced.

DISCUSSIONS AND CONCLUSION

The present results on phantoms show the feasibility of separating two positron emitters in PCT, but image noise is enhanced in the separated images. The amount of enhancement depends on the time duration of the projection measurements, the ratio of the two half-lives,

TABLE 1. COMPARISON OF QUANTITATIVE VALUES IN DOUBLE-TRACER IMAGES WITH THOSE IN CONTROLS

Experiment 1			Experiment 2			Experiment 3		
Images	N-13 compartment	F-18 compartments	Images	Ga-68 compartments	Cu-64 compartments	Images	Center compartment	Side compartments
N-13 by DTT‡	4523[a] (233)*	213† (182) 61 (103)	Ga-68 by DTT	12964 (1104)	112 (758)	Attenuation coef. from DTT	0.004 (0.007)	0.091 (0.009)
F-18 by DTT	54 (158)	3018 (115) 2440 (74)	Cu-64 by DTT	341 (806)	13918 (934)	Attenuation coef. from control	0.003 (0.002)	0.090 (0.003)
F-18 Control	105 (58)	2998 (17) 2394 (35)	Cu-64 Control	−9 (209)	14034 (483)	N-13 by DTT	189 (728)	2546† (942) 3340 (1035)
Sum of N-13 and F-18	4575 (125)	3144 (100) 2540 (42)	Sum of Ga-68 and Cu-64	13304 (412)	14030 (528)	N-13 using ACFs from control	218 (508)	2376 (665) 3152 (662)
Initial image	4220 (108)	3177 (83) 2580 (49)	Initial image	12775 (336)	13767 (316)	N-13 control	200 (121)	2509 (147) 3450 (169)

(a) Values in table have the same unit for all images in each experiment, but the unit is arbitrary except for attenuation coefficient, which has the dimension cm^{-1}. Comparison of values by DTT against those of control indicate the effectiveness of the double-tracer technique. In experiments 1 and 2, the validity of the values for N-13 and Ga-68 can be checked by comparing the sum images with the initial images.

* Values in the parentheses are s.d. of pixel values in the regions.

† First value corresponds to compartment on the left; second value that on the right.

‡ Double-tracer technique

and the relative radioactivity levels of the tracer. Usually the noise enhancement is tolerable if the half-life ratio is larger than 5 and the scan measurement time is longer than the smaller half-life. Additional studies will doubtless help to optimize the signal-to-noise ratios in the images. In the case of the combined transmission and emission scans, the boundary method for attenuation correction (*12*), which can reduce the noise level in the transmission measurements, is potentially useful in limiting the noise enhancement of the double-tracer technique. We used this method in our third study, but the noise improvement was not dramatic (CV fell from about 30% to 20%), due to the lower relative radioactivity

FIG. 5. Images of attenuation coefficients of a phantom in combined transmission and emission study. At left is reconstruction from transmission measurements separated out by double-tracer technique. At right is control obtained from regular PCT transmission scan of phantom after all its radioactivity had decayed. Attenuation coefficients of water as obtained from these two images are also found approximately equal (μ = 0.090 cm^{-1}).

FIG. 6. Images of phantom in combined transmission and emission study. Center image was reconstructed from N-13 radioactivity separated by double-tracer technique. Attenuation correction factors were from separated Ga-68 transmission data in same study. Image at left was from same N-13 data, but attenuation correction factors were derived from control transmission scan at right in Fig. 5. At right is control N-13 image. Except for difference in noise levels, the three images give same distribution of N-13. Similar noise patterns at left and center indicate that dominant source of noise was from N-13 data, which are common to both, rather than from ACFs, which were not common.

level in the phantom than in the transmission ring (~17.5 million counts vs. ~3.5 million). After processing by the double-tracer technique, the percent noise level was higher in the emission data than in the transmission data. Thus final image noise was dominated by the noise in the emission data, which is outside the capability of the boundary method (*12*). If the phantom has a higher radioactivity level than that in the transmission ring, the boundary method will be much more effective in controlling noise.

The double-tracer technique presented here assumes that the time variation of the tracer distributions is only due to the nuclides' physical decay. In biological clearances or uptakes, this assumption will be violated and the technique will incur errors. The size of this error will depend on the rate of redistribution relative to physical decay. Conceptually, this tracer redistribution problem can be taken into account by including a linear term in the coefficients of the exponential components of $m(r,\theta,t)$. That is, one can assume that the time function of each projection has the following form

$$m(r,\theta,t) = [m_A(r,\theta) + S_A(r,\theta)t]e^{-\lambda_A t} + [m_B(r,\theta) + S_B(r,\theta)t]e^{-\lambda_B t}, \quad (5)$$

and that it can estimate all four parameters m_A, S_A, m_B and S_B simultaneously. The parameters S_A and S_B correspond to the sum along the projection line $l(r,\theta)$ of the rates of redistributions of f_A and f_B, respectively. In other words, the parameters S_A and S_B are also projections that can be used to reconstruct images of the redistribution rates of the tracers. However, the noise-enhancement problem is expected to be worse because two more parameters (S_A and S_B) will need to be estimated from the projection data.

Higher photon counts can, of course, palliate the noise problem, but these demand larger tracer doses and/or higher detection efficiency in the PCT, together with improved count-rate capability to minimize dead-time problems (*13*).

Systematic errors as well as high random noise could degrade the estimated values of m_A and m_B, and their effects will need to be explored further.

In the present technique, the radioactivities of the two nuclides are separated using the time function of the projection measurements. Alternatively, one could first reconstruct images of the sum of the two nuclides at various times and then separate the two emitting components in each pixel by using the time variation of the reconstructed image values. However, this alternative procedure cannot be used easily for combined transmission and emission scans, and is expected to require more computing time and to have more serious noise problems.

Although this double-tracer method is currently in its infancy, we expect it to be useful in situations where the advantages of simultaneously studying two positron tracers outweigh the technical difficulties. For example, in PCT cardiac studies, zones of increased glycolysis (indicated by F-18 FDG uptake) and decreased perfusion (indicated by N-13 ammonia) potentially provide evidence of reversible ischemic myocardial tissue (*14*). Because of the regional variation in myocardial thickness and the partial-volume effect (*15*), the PCT images of myocardium are very position-dependent, and it is essential that the distributions of FDG and ammonia be compared in the same cross section of the heart. The current practice of scanning a patient for FDG at least an hour after the ammonia scan (*16,17*) brings on severe repositioning problems. With the double-tracer technique the two distributions will be measured concurrently. The total patient study time would also be shortened because studying with two tracers in sequence requires the first tracer to decay away before the second is started.

For combined transmission and emission scans, the technique can completely eliminate the problem of patient movement in between, which can introduce significant artifacts in PCT images (*6*). In this application, the boundary method for attenuation correction (*12*) can reduce the noise in the transmission measurements. However, before the various problems associated with the double-tracer technique are clearly understood, the method should be used cautiously. We expect that some practical guidelines or solutions will be developed soon, to enhance the usefulness of the technique.

FOOTNOTES

* EGG/ORTEC Inc., Oak Ridge, TN.

ACKNOWLEDGMENT

We thank Joann Miller, Ron Sumida, and Francine Aquilar for their assistance in performing the tomographic scans; Dr. N. MacDonald and the UCLA medical cyclotron staffs for producing the positron emitters; Robin Townsend for typing the manuscript, and Lee Griswold for preparing the illustrations.

This work was supported by DOE Contract DE-AM03-76-SF-0012, NIH Grant R01-GM-24839-01 and USPH Grant 515654-01.

APPENDIX: DERIVATION OF ESTIMATION EQUATIONS FOR DOUBLE TRACER TECHNIQUE

For two radionuclides with decay constants λ_A and λ_B: If their radioactivity levels at time $t = 0$ are m_A and m_B, the sum of the two radioactivities at time t_i will be

$$m(t_i) = m_A e^{-\lambda_A t_i} + m_B e^{-\lambda_B t_i} \; (i = 1,\ldots,n). \quad (A1)$$

Let z_i be the value actually measured at time t_i. If m_A and m_B are not known and need to be estimated from the values of z_i, we need to find a set of estimates, $\hat{m}_A$ and $\hat{m}_B$, that would best match the measurements z_i. Applying the method of least squares (18), we want $\hat{m}_A$ and $\hat{m}_B$ to minimize the cost function $G = \Sigma_i [z_i - m(t_i)]^2$. By setting to zero the partial derivatives of G with respect to m_A and m_B, one can solve for $\hat{m}_A$ and $\hat{m}_B$ in terms of z_i as

$$\hat{m}_A = \frac{1}{D}\left[\left(\sum_i z_i e^{-\lambda_A t_i}\right)\left(\sum_i e^{-2\lambda_B t_i}\right) - \left(\sum_i z_i e^{-\lambda_B t_i}\right)\left(\sum_i e^{-(\lambda_A+\lambda_B)t_i}\right)\right]$$

$$\hat{m}_B = \frac{1}{D}\left[\left(\sum_i z_i e^{-\lambda_B t_i}\right)\left(\sum_i e^{-2\lambda_A t_i}\right) - \left(\sum_i z_i e^{-\lambda_A t_i}\right)\left(\sum_i e^{-(\lambda_A+\lambda_B)t_i}\right)\right] \quad \text{(A2)}$$

where

$$D = \left(\sum_i e^{-2\lambda_A t_i}\right)\left(\sum_i e^{-2\lambda_B t_i}\right) - \left(\sum_i e^{-(\lambda_A+\lambda_B)t_i}\right)^2$$

Given Possion noise, the noise variance in the measurements of z_i is proportional to z_i (*19*), so each of the squared terms in the cost function G should be weighted by the inverse of the noise variance (i.e., weighted by $1/z_i$) (*20*). In other words, the cost function G should be $\Sigma_i [z_i - m(t_i)]^2/z_i$, and the estimates $\hat{m}_A$ and $\hat{m}_B$ could be expressed as

$$\hat{m}_A = \frac{1}{E}\left[\left(\sum_i e^{-\lambda_A t_i}\right)\left(\sum_i e^{-2\lambda_B t_i}/z_i\right) - \left(\sum_i e^{-\lambda_B t_i}\right)\left(\sum_i e^{-(\lambda_A+\lambda_B)t_i}/z_i\right)\right]$$

$$\hat{m}_B = \frac{1}{E}\left[\left(\sum_i e^{-\lambda_B t_i}\right)\left(\sum_i e^{-2\lambda_A t_i}/z_i\right) - \left(\sum_i e^{-\lambda_A t_i}\right)\left(\sum_i e^{-(\lambda_A+\lambda_B)t_i}/z_i\right)\right] \quad \text{(A3)}$$

where

$$E = \left(\sum_i e^{-2\lambda_A t_i}/z_i\right)\left(\sum_i e^{-2\lambda_B t_i}/z_i\right) - \left(\sum_i e^{-(\lambda_A+\lambda_B)t_i}/z_i\right)^2$$

In the above equation, the noise variance of each measurement was assumed to be proportional to z_i, whereas, rigorously, for Poisson noise, the noise variance is proportional to $m(t_i)$. However, if $1/m(t_i)$ is used for the weighting, the estimation equations are much more complex, and the estimates $\hat{m}_A$ and $\hat{m}_B$ will need to be solved by iterative procedures. For the data presented in this report, no significant difference in results was observed by changing the weighting factors in the cost function G.

REFERENCES

1. BEN-PORATH M, CLAYTON G, KAPLAN E: Modification of a multi-isotope color scanner for multi-purpose scanning, *J. Nucl Med* 8:411-425, 1967
2. BLANQUET PC, BECK CR, FLEURY J, PALAIS CJ: Pancreas scanning with Se-75-Selenomethionine and Au-198 using digital-data-processing techniques. *J Nucl Med* 9:486-488, 1968
3. BURAGGIL GL, LAURINI, R, RODARI A, et al: Double-tracer scintigraphy with 67Ga Citrate and 99mTc Sulfur colloid in the diagnosis of hepatic tumors. *J Nucl Med* 17: 369-373, 1976
4. DHAWAN VM, SZIKLAS JJ, SPENCER RP, et al: Computerized double-tracer subtraction scanning with Ga-67 Citrate in inflammatory diseases. *J Nucl Med* 19:1297-1300, 1978
5. RITCHIE JL, HAMILTON GW, GOULD KL, et al: Myocardial imaging with indium-113m and Technetium-99m macroaggregated albumin. *Am J Cardiol* 35:380-389, 1975
6. HUANG S-C, HOFFMAN EJ, PHELPS ME, et al: Quantitation in positron emission computed tomography: 2. Effects of inaccurate attenuation correction. *J Comput Assist Tomog* 3:804-814, 1979
7. RAMACHANDRAN GN, LAKSHMINARAYANAN AV: Three-dimensional reconstruction from radiographs and electron micrographs: Application of convolutions instead of Fourier transforms. *Proc Nat Acad Sci* 68:2236-2240, 1971
8. SHEPP LA, LOGAN BF: The Fourier reconstruction of a head section. *IEEE Trans Nucl Sci* NS-21:21-43, 1974
9. PHELPS ME, HOFFMAN EJ, HUANG S-C, et al: ECAT A new computerized tomograph imaging system for positron-emitting radiopharmaceuticals. *J Nucl Med* 19:635-647, 1978
10. HOFFMAN EJ, PHELPS ME, HUANG S-C, et al: A new tomograph for quantitative positron computed tomography of the brain. *IEEE Trans Nucl Sci* NS-28:99-103, 1981
11. PHELPS ME, HOFFMAN EJ, MULLINI NU, et al: Some performance and design characteristics of PETT III. In *Reconstruction Tomography in Diagnostic Radiology and Nuclear Medicine*. Ter-Pogossian MM, Phelps ME, Brownell GL., et al., Eds. University Park Press, Baltimore, 1977, pp 371-392
12. HUANG S-C, CARSON R, PHELPS ME, et al: A boundary method for attenuation correction in positron computed tomography. *J Nucl Med* 22:627-637, 1981
13. HOFFMAN EJ, HUANG S-C, PHELPS ME, et al: Quantitation in Positron emission computed tomography: 4. Effect of accidental coincidences. *J Comput Assist Tomog* 5:391-400, 1981
14. MARSHALL RC, SCHELBERT HR, TILLISCH JH, et al: Identification of ischemic myocardium using 18-fluorodeoxyglucose, N-13-ammonia and positron computed tomography. *J Nucl Med* 22:p39, 1981 (abst)
15. HOFFMAN EJ, HUANG S-C, PHELPS ME: Quantitation in positron emission computed tomography: 1. Effect of object size. *J Comput Assist Tomogr* 3:299-308, 1979
16. PHELPS ME, HUANG S-C, HOFFMAN EJ, et al: Tomographic measurement of local cerebral glucose metabolic rate in humans with (F-18)2-fluoro-2-deoxy-D-glucose: Validation of method. *Ann Neurol* 6:371-388, 1979
17. HUANG S-C, PHELPS ME, HOFFMAN EJ, et al: Noninvasive determination of local cerebral metabolic rate of glucose in man. *Am J Physiol* 238:E69-E82, 1980
18. HOEL PG: Introduction to Mathematical Statistics, 4th ed., Chap. 7, Wiley, New York, 1971
19. SORENSON JA, PHELPS ME, *Physics in Nuclear Medicine*, Chap. 6, Grune and Stratton, New York, 1980
20. DRAPER N, SMITH H: *Applied Regression Analysis*, Wiley, New York, 1966, pp 79-81